2003

Mechanisms for the Oxonolysis of Ethene and Propene: Reliability of Quantum Chemical Predictions

Wai-To Chan
Wilfrid Laurier University

Ian P. Hamilton
Wilfrid Laurier University, ihamilton@wlu.ca

Mechanisms for the ozonolysis of ethene and propene: Reliability of quantum chemical predictions

Wai-To Chan and I. P. Hamilton[a)]
Department of Chemistry, Wilfrid Laurier University, Waterloo, Canada N2L 3C5

(Received 10 July 2002; accepted 29 October 2002)

Reactions of ozone with ethene and propene leading to primary ozonide (concerted and stepwise ozonolysis) or epoxide and singlet molecular oxygen (partial ozonolysis) are studied theoretically. The mechanism of concerted ozonolysis proceeds via a single transition structure which is a partial diradical. The transition structures and intermediates in the stepwise ozonolysis and partial ozonolysis mechanisms are singlet diradicals. Spin-restricted and unrestricted density functional methods are employed to calculate the structures of the closed-shell and diradical species. Although the partial diradicals exhibit moderate to pronounced instability in their RDFT and RHF solutions, RDFT is required to locate the transition structure for concerted ozonolysis. Spin projected fourth-order Møller–Plesset theory (PMP4) was used to correct the DFT energies. The calculated pre-exponential factors and activation energies for the concerted ozonolysis of ethene and propene are in good agreement with experimental values. However, the PMP4//DFT procedure incorrectly predicts the stepwise mechanism as the favored channel. UCCSD(T) predicts the concerted mechanism as the favored channel but significantly overestimates the activation energies. RCCSD(T) is found to be more accurate than UCCSD(T) for the calculation of the concerted mechanism but is not applicable to the diradical intermediates. The major difficulty in accurate prediction of the rate constant data for these reactions is the wide range of spin contamination for the reference UHF wave functions and UDFT solutions across the potential energy surface. The possibility of the partial ozonolysis mechanism being the source of epoxide observed in some experiments is discussed. [DOI: 10.1063/1.1531104]

I. INTRODUCTION

Initiation of the degradation of tropospherically abundant nonmethane hydrocarbon species containing alkenic double bonds, typically isoprene and terpene, occurs via attack by one of the atmospheric oxidants: the hydroxyl radical OH, the nitrate radical NO_3 or ozone, O_3, a singlet diradical.[1] The dominant pathway for the reaction of ozone and alkene is believed to be the Criegee mechanism (shown here for ethene)[2]

$$C_2H_4 + O_3 \rightarrow \text{cyc-}CH_2O_3CH_2 \rightarrow \text{products}.$$

The first step of this mechanism is the highly exothermic cycloaddition of O_3 to the alkene double bond giving the primary ozonide cyc-$CH_2O_3CH_2$, a π bridge complex which has a five-membered ring structure. A comprehensive review of kinetic studies of the gas phase reactions between ozone and a variety of organic compounds including alkenes has been given by Atkinson and Carter.[3] More recently, the fragmentation of the ozonide and subsequent reactions to form a variety of products has been reviewed by Horie and Moortgat.[4] Recent theoretical studies of ozone–alkene reactions have mainly focussed on elucidation of the reaction pathway for the formation of OH by means of quantum chemical calculations of potential energy surface features.[5–9]

The objective of the present study is to examine the reliability of quantum chemical prediction of the reaction mechanism of gas-phase alkene ozonolysis through comparison of computed and experimental values for the pre-exponential factor and activation energy. For the ozonolysis of ethene, the mechanisms considered, R1 (concerted), R2 (stepwise), and R3 (partial), are summarized as

$$\text{R1} \quad C_2H_4 + O_3 \xrightarrow{\text{TS1}} \text{cyc-}CH_2O_3CH_2,$$

$$\text{R2a} \quad C_2H_4 + O_3 \xrightarrow{\text{TS2a}} CH_2CH_2O_3(2),$$

$$\text{R2b} \quad CH_2CH_2O_3(2) \xrightarrow{\text{TS2b}} \text{cyc-}CH_2O_3CH_2,$$

$$\text{R3a} \quad C_2H_4 + O_3 \xrightarrow{\text{TS3a}} CH_2CH_2O_3(3),$$

$$\text{R3b} \quad CH_2CH_2O_3(3) \xrightarrow{\text{TS3b}} \text{cyc-}CH_2OCH_2 + {}^1O_2.$$

In R1, shown in Fig. 1, O_3 reacts with ethene in a concerted fashion via a single transition structure, TS1, to form cyc-$CH_2O_3CH_2$. In R2, shown in Fig. 2, O_3 reacts with ethene in a stepwise fashion via two transition structures. In R2a, the terminal O atom in O_3 binds to a C atom in ethene via TS2a, to form a singlet diradical intermediate denoted as $CH_2CH_2O_3(2)$ which has a partially open five-membered ring structure. In R2b, ring closure of $CH_2CH_2O_3(2)$ occurs

a)Member, Guelph-Waterloo Center for Graduate Work in Chemistry. Electronic mail: ihamilto@wlu.ca

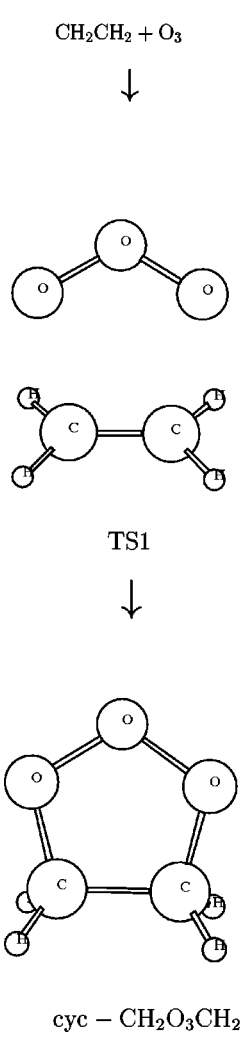

FIG. 1. Concerted ethene ozonolysis: $C_2H_4 + O_3 \xrightarrow{TS1}$ cyc-$CH_2O_3CH_2$. BH&HLYP/6-31+G(d), P(R)MP4/6-311+G(2d,p)//DFT, and U(R)CCSD(T)/6-311+G(2d,p)//DFT results. Bond distances in Å. E, total electronic energy; H_0, total enthalpy at zero-temperature (E+unscaled DFT zero-point vibrational energy); S_{298}, total entropy at 298.15 K. E, H_0, and S_{298} set to zero for $C_2H_4+O_3$ as reference values. *Relative to the RCCSD(T) energy of ozone. Also see Ref. 35.

via TS2b to form cyc-$CH_2O_3CH_2$. Evidence for the concerted pathway is based on the observed reaction stereospecificity and the large negative entropy of activation indicative of a constrained transition structure.[10]

A possible competing mechanism (postulated by Criegee[2]) is R3, shown in Fig. 3. In R3a, a σ-adduct $CH_2CH_2O_3(3)$ is formed which has a less constrained and more open structure than $CH_2CH_2O_3(2)$. In R3b, dissociation of the CH_2CH_2O–OO bond leads to the formation of oxirane (ethylene oxide) and singlet molecular oxygen. Formation of epoxide has been observed in small yield in the gas-phase ozonolysis of several alkenes but the source of this species was unclear.[11]

To our knowledge, no theoretical studies of R2 and R3 including characterization of the singlet diradical intermediates and transition structures have been reported. Among recent theoretical examinations of stepwise versus concerted mechanisms involving singlet diradicals, one study concerns the reaction between ozone and acetylene.[12] Based on prediction of the reaction rate constant for the concerted mechanism, the experimental value of the pre-exponential factor indicative of a stepwise mechanism was disputed. In another study, a stepwise mechanism was predicted for the reaction between singlet molecular oxygen and ethene involving a diradical intermediate $CH_2CH_2O_2$.[13]

For the ozonolysis of propene, mechanisms parallel to R1–R3, R4 (concerted), R5 (stepwise), and R6 (partial), are summarized as

$$\text{R4}\quad CH_3CHCH_2 + O_3 \xrightarrow{TS4} \text{cyc-}CH_3CHO_3CH_2,$$

$$\text{R5a}\quad CH_3CHCH_2 + O_3 \xrightarrow{TS5a} CH_3CHCH_2O_3(5),$$

$$\text{R5b}\quad CH_3CHCH_2O_3(5) \xrightarrow{TS5b} \text{cyc-}CH_3CHO_3CH_2,$$

$$\text{R6a}\quad CH_3CHCH_2 + O_3 \xrightarrow{TS6a} CH_3CHCH_2O_3(6),$$

$$\text{R6b}\quad CH_3CHCH_2O_3(6) \xrightarrow{TS6b} \text{cyc-}CH_3CHOCH_2 + {}^1O_2.$$

II. METHOD

Prediction of radical–molecule reactivities can generally be accomplished by applying various methods, most commonly density functional theory (DFT) or second-order Møller–Plesset perturbation theory (MP2) to search for and characterize the reactants, products, and transition structures in the potential energy surface (PES). This is followed by refinement of the DFT/MP2 estimates of reaction and activa-

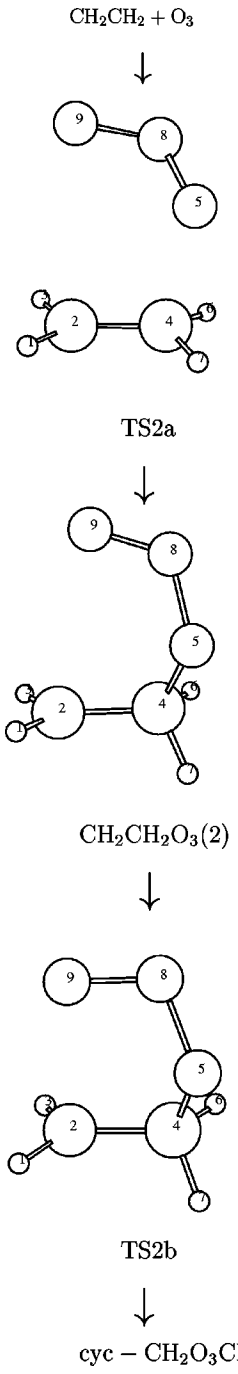

			UDFT	PMP4	UCCSD(T)
O9–O8	1.274	E	+7.3 Kcal/mole	+3.5	+10.2
O8–O5	1.344	H_0	+8.4 Kcal/mole	+4.6	+11.2
O5–C4	1.981	S_{298}	-32.9 cal/mole/K		
O9–C2	2.974				
C4–C2	1.368				
O9-O8-O6	112.3°				

$\omega_{1-3} = 481i,\ 70,\ 124\ cm^{-1}$

			UDFT	PMP4	UCCSD(T)
O9–O8	1.267	E	-9.7 Kcal/mole	-6.8	-2.4
O8–O5	1.426	H_0	-7.8 Kcal/mole	-4.9	-0.5
O5–C4	1.439	S_{298}	-32.9 cal/mole/K		
O9–C2	2.880				
C4–C2	1.478				
O9-O8-O5	110.5°				

$\omega_{1-3} = 92,\ 141,\ 166\ cm^{-1}$

			UDFT	PMP4	UCCSD(T)
O9–O8	1.285	E	-8.9 Kcal/mole	-9.8	-3.5
O8–O5	1.414	H_0	-6.6 Kcal/mole	-7.5	-1.2
O5–C4	1.443	S_{298}	-39.0 cal/mole/K		
O9–C2	2.389				
C4–C2	1.479				
O9-O8-O5	108.2°				

$\omega_{1-3} = 248i,\ 182,\ 345\ cm^{-1}$

FIG. 2. Stepwise ethene ozonolysis: $C_2H_4 + O_3 \xrightarrow{\text{TS2a}} CH_2CH_2O_3(2) \xrightarrow{\text{TS2b}}$ cyc-$CH_2O_3CH_2$.

tion energies using a higher-level method such as MP4 or coupled-cluster theory (CCSD(T)). We now address some limitations of these methods pertinent to the present study.

The transition structures and intermediates for the stepwise pathway are singlet diradicals. Correct description of a singlet diradical electronic state requires the reference Hartree–Fock wave function for MP2 and DFT to be spin-unrestricted (U) because the spin-restricted (R) solution is unstable towards spin-symmetry breaking. In formally closed-shell systems, the onset of such RHF/UHF or RDFT/UDFT instability also occurs upon distortion from the equilibrium geometry. Spin contamination of the UHF/UDFT solution and the degree of instability of the RHF/RDFT solution are expected to be small in a region near the point of instability. Hence RMP2 (based on RHF) and RDFT are generally adequate for calculation of PES features. However, for the diradicals in the present study, both the UHF and UDFT solutions exhibit severe spin contamination due to heavy mixing of triplet and higher spin states.

DFT is known to be less susceptible to spin contamination than MPn.[14] This makes UDFT a more reliable method than UMPn provided that the degree of spin contamination is not substantial enough to cause significant distortion of the PES. A correlation method beyond UMPn, such as UCCSD(T), is more effective for correction of spin-contaminated wavefunctions but large-scale UCCSD(T) cal-

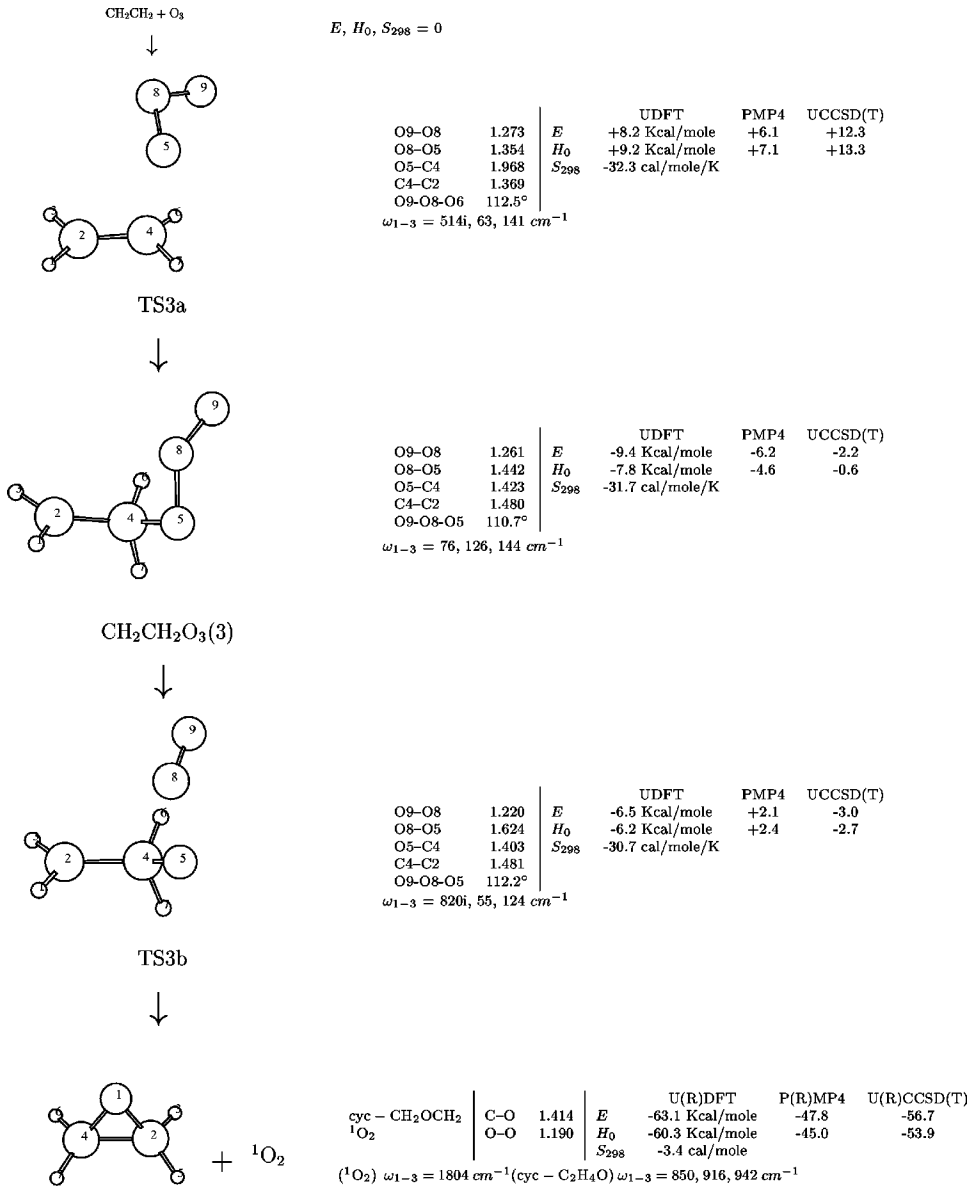

FIG. 3. Partial ethene ozonolysis: $C_2H_4 + O_3 \xrightarrow{TS3a} CH_2CH_2O_3(3) \xrightarrow{TS3b}$ cyc-$CH_2OCH_2 + {}^1O_2$.

culations for characterization of PES features are impractical. Alternately, spin-projection can be applied to improve barrier heights obtained from spin-contaminated UDFT solutions.[15] Spin-projected DFT was shown to result in further degradation of the UDFT PES[16] but spin-projected MP4 (PMP4) should provide improvement. Although the CCSD(T) method is expected to be more reliable,[17] comparison between PMP4 and CCSD(T) is included in this study to test whether MP4 is sufficiently reliable to be an alternate procedure.

The transition structure for the concerted pathway (R1) is not formally a diradical but occurs in a region of the PES near the onset of a restricted/unrestricted instability intermediate between the closed-shell ozonide and the TS. The ozonide is well described by either RHF or RDFT. However, upon distortion of the C–O bonds, instability of the restricted solution towards spin-symmetry breaking (and spatial-symmetry breaking for ethene/ozone for which the TS is symmetric) sets in. To avoid the symmetry breaking, a search of the concerted TS structure must be carried out with RDFT since this point is absent on the PES generated by UDFT. Such discontinuity between the restricted and unrestricted PES at the point of symmetry breaking renders energetic comparison of the RDFT concerted TS structure and the UDFT diradical structure meaningless as these are stationary points on two different PESs.

The effect of symmetry breaking on the wavefunction can be circumvented by using the complete active space self-consistent-field (CASSCF) approach to formulate a multiconfiguration wavefunction that yields a single PES for both the concerted and stepwise TSs but large-scale CASSCF calculations for characterization of PES features are impractical. Moreover, a CASSCF study could yield an inaccurate PES[18] due to overemphasis of static electron correlation (the effect of allowing the wavefunction to include more than one configuration). Correction of the CASSCF wavefunction for dy-

TABLE I. Equilibrium geometry and harmonic vibrations of ground state ozone by restricted and unrestricted methods.[a]

Method	R_e/Å	θ/deg	$\omega_1(a_1)$	$\omega_2(a_1)$	$\omega_3(b_2)$
RBLYP/6-31+G(d)	1.298	118.0	1133	672	1003
UBLYP/6-31+G(d)	/	/	/	/	/
RB3LYP/6-31+G(d)	1.263	118.2	1258	733	1220
UB3LYP/6-31+G(d)	1.285	116.3	1032	698	1085
RBH&HLYP/6-31+G(d)	1.231	118.5	1396	793	1407
UBH&HLYP/6-31+G(d)	1.282	114.0	1113	713	1172
RMP4/6-311+G(2d)	1.301	117.6	1086	684	1603
UMP4/6-311+G(2d)	1.307	113.9	1010	663	1021
RQCISD/6-311+G(2d)	1.260	117.9	1230	736	933
UQCISD/6-311+G(2d)	1.295	115.2	979	683	971
RCCSD(T)/6-311+G(2d)	1.282	117.1	1129	702	1014
UCCSD(T)/6-311+G(2d)	1.280	116.9	1026	698	1093
RBD(T)/6-311+G(2d)	1.281	117.1	1135	696	1120
UBD(T)/6-311+G(2d)	/	/	/	/	/
Experiment (Refs. 31, 32)	1.272	116.8	1135	716	1089
CISD[TQ] (Ref. 33)	1.281	116.7	1166	716	1138

[a]Note: Frequencies in cm^{-1}.

namic correlation using multireference perturbation theory is required to give reliable results.[19] Currently, the application of such an approach is not feasible.

In light of these difficulties, quantitative predictions are not to be expected from the present study. However, we contend that even qualitative predictions could aid in the interpretation of experimental data through correlation between the calculated and experimental rate constant data.

III. PROCEDURE

The GAUSSIAN 98 program package[20] was employed to perform the DFT and *ab initio* calculations reported here.

The choice of a DFT method capable of reliable prediction of transition state properties is crucial for identification of the mechanistic pathway through kinetic characterization. Accurate prediction of activation energies has been shown for three hybrid functionals; BH&HLYP,[21,22] MPW1K,[23] and KMLYP,[24] with the latter two methods shown to be more accurate than BH&HLYP for their studies. On the other hand, BH&HLYP has been shown to provide a reliable estimate of the activation energy for the concerted dissociation of *s*-trioxane ($(CH_2O)_3$) to CH_2O (Ref. 25) and for the dissociative cyclization of alkyl hydroperoxyl radical to epoxide and hydroxyl radical,[26] two reactions bearing some degree of similarity to the concerted and partial ozonolysis pathways in this study. Calibration data of the performance of DFT methods for characterization of diradical transition states is lacking. It has been suggested[27] that because of Hartree–Fock mixing in the hybrid functionals, pure nonlocal DFT methods such as BLYP are more suitable. This contention is compromised by a recent analysis[28] of the correlation effects covered by both types of DFT methods which concluded that unrestricted DFT methods are more accurate when carried out with the hybrid functionals. For this study the BH&HLYP/6-31+G(d) method was employed for geometry optimization and harmonic analysis of the equilibrium and transition structures in the ozonolysis pathways. The choice of this method is based on our study of the performance of the BH&HLYP, B3LYP, and BLYP methods on ozone and the two diradical intermediates for the stepwise pathway of ethene ozonolysis.

For ethene ozonolysis all diradical transition structures and intermediates, TS2a,2b,3a,3b, $CH_2CH_2O_3(2)$ and $CH_2CH_2O_3(3)$, O_3 and $^1O_2$ were characterized by geometry optimization and harmonic analysis using the UDFT method. TS1 (a partial diradical) and the closed-shell species, ethene, oxirane and the primary ozonide were treated by RDFT. Activation barriers and energy changes of R1–R3 were refined by PMP4 and UCCSD(T) with the basis set 6-311 +G(2d,p). The activation barrier and energy change of R1 was also computed with RCCSD(T). The UDFT and UHF solutions were obtained using the guess=mix keyword option to destroy spin and spatial symmetries followed by the stable=opt option to verify the stability of the solution. Because heavy spin contamination of the reference UHF wave functions of the diradicals and TS1 renders the UMP4 energies unreliable, the PMP4 energies are reported. To assess the accuracy of the CCSD(T) data, T_1 diagnostic values[29] were computed for the R and UCCSD wave functions. A value of T_1 below 0.02 is indicative of a CCSD(T) result closely approximating the full CI limit.

High pressure limiting rate constants for each reaction step were calculated by standard transition state theory (TST). For example, the TST expression for R1,

$$k_1 = \frac{k_b T}{h} \frac{Q_{TS1}}{Q_{C_2H_4} Q_{O_3}} \exp(-\Delta E^{\ddagger}/RT),$$

was evaluated from the computed total partition functions of the $C_2H_4+O_3$ reactants and TS1 and the barrier height for a series of temperatures between 235 and 362 K, the experimental range of Herron and Huie.[30] The calculated rate constants were fit to a $\ln k_1$ versus 1/T plot and the pre-exponential factor, A, and activation energy, E_{act} were derived from the intercept and slope of this plot to obtain the Arrhenius expression: $k_1 = A \exp(-E_{act}/RT)$.

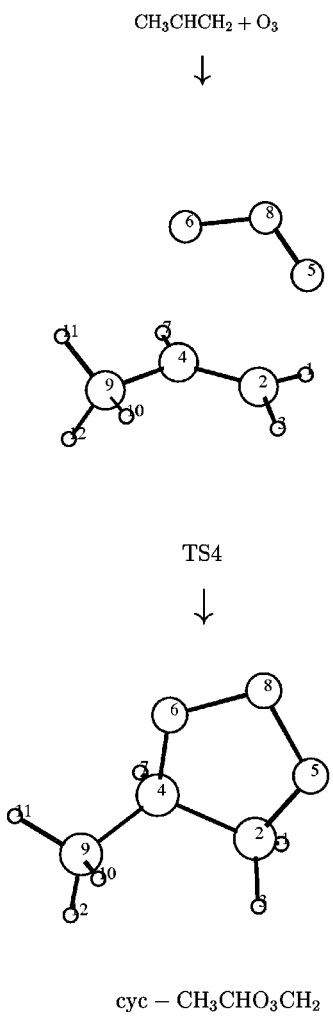

FIG. 4. Concerted propene ozonolysis: $CH_3CHCH_2+O_3 \xrightarrow{TS4}$ cyc-$CH_3CHO_3CH_2$. E, H_0, and S_{298} set to zero for $CH_3CHCH_2+O_3$ as reference values.

For propene ozonolysis, parallel DFT and MP4 calculations were performed for R4–R6. RCCSD(T) was employed to compute R4. Application of UCCSD(T) was excluded because of prohibitive external storage requirements.

IV. RESULTS AND DISCUSSION

A. Calibration of restricted and unrestricted methods

The diradical character of both ozone and the TS in the concerted ozonolysis pathway is incomplete. It is therefore expected that a sufficiently high level single-reference *ab initio* method is capable of correcting the absence of diradical character of a RHF or the spin contamination of a UHF reference wave function, yielding similarly accurate molecular properties. Likewise, an accurate RDFT method is expected to be stable towards symmetry breaking for a partial diradical. Accurate calculations of the properties of ground state ozone have proven to be a difficult challenge to theory and even a qualitatively correct prediction of the order of the vibrations requires application of methods beyond CISD (Ref. 33). To assess the reliability of the methods typically employed we carried out a performance calibration of the *ab initio* methods: MP4, QCISD, CCSD(T), BD(T), and DFT methods: BLYP, B3LYP, and BH&HLYP in both their spin-restricted and unrestricted formalism against experimental[31,32] and theoretical[33] data on the geometry and harmonic vibrational frequencies of ozone.

From Table I, comparision of the results of the series of RDFT and UDFT methods and the reference data reveal RBLYP and RB3LYP to be the only methods correctly predicting the antisymmetric (b_2) stretching frequency to be lower than the symmetric (a_1) stretching frequency. RBLYP is stable towards symmetry breaking and no UBLYP solution is found at the equilibrium geometry. The absolute errors of the predicted vibrations of both RB3LYP and RBH&HLYP are considerably larger than RBLYP. Application of the U method results in more substantial improvement over the R method for BH&HLYP than for B3LYP but the order of the stretching frequencies is incorrect.

Of the *ab initio* wave-function-based methods, RMP4 predicts a spuriously large antisymmetric stretching frequency of 1603 cm^{-1}. The UMP4 predictions are better but the errors remain significant. Beyond MP4, both UHF and RHF based QCISD predict the correct order of the two stretching vibrations. Surprisingly, UCCSD(T) predicts the incorrect order. The overall agreement of both the R and UCCSD(T) results with the reference data is nonetheless better than that for R and UQCISD indicating the importance of the inclusion of triple excitations for a proper description of

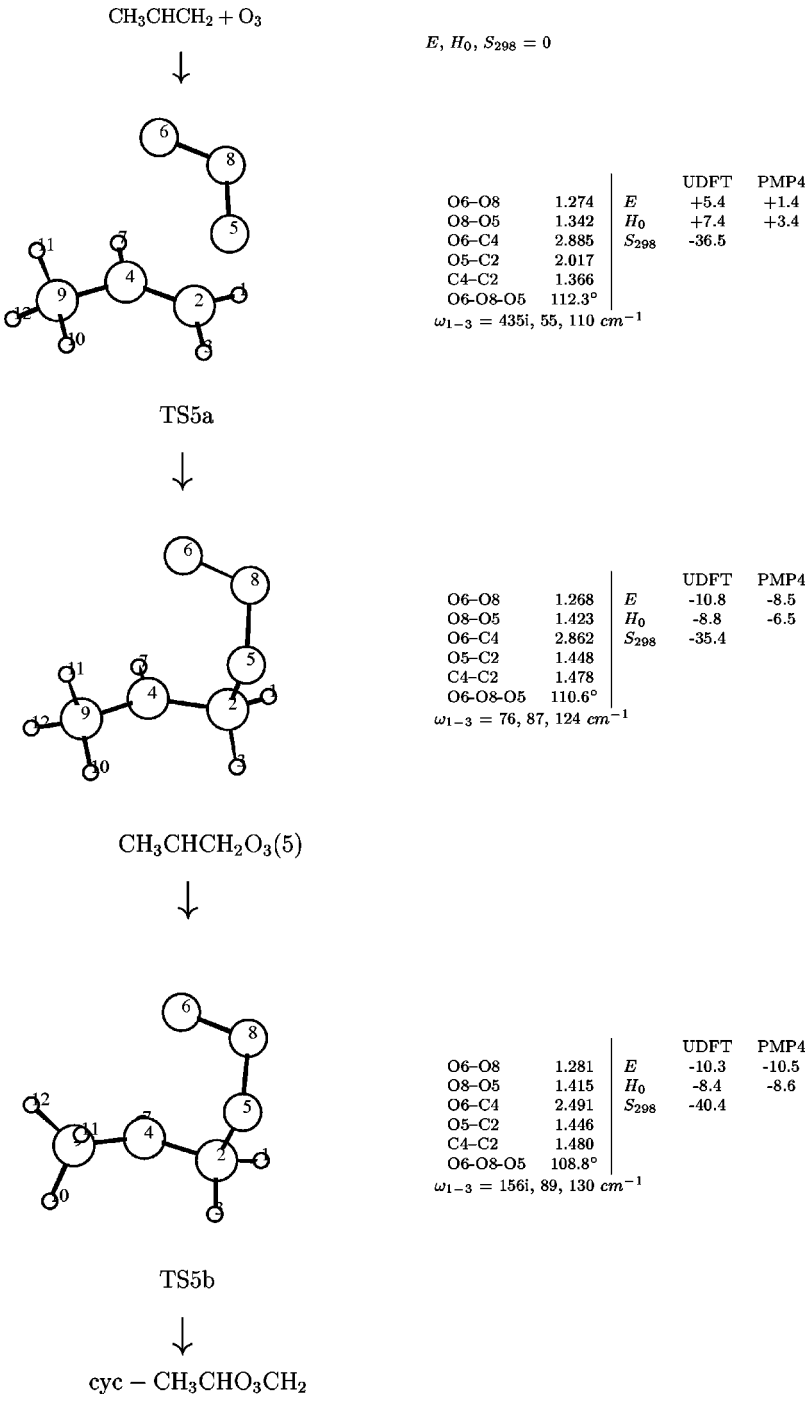

FIG. 5. Stepwise propene ozonolysis: $CH_3CHCH_2 + O_3 \xrightarrow{TS5a} CH_3CHCH_2O_3(5) \xrightarrow{TS5b}$ cyc-$CH_3CHO_3CH_2$.

the partial diradical. The diagnostic value (see Appendix) of the RCCSD wave function (0.029) is significantly lower than that for the UCCSD wave function (0.061). This is consistent with the improved accuracy of the R methods at the CCSD(T) level. RBD(T) gives results very close to RCCSD(T) except for the b_2 stretching vibration which is significantly more accurate. Geometry optimization with the UBD(T) method was abandoned because it converged to a region of the PES where the UHF wave function collapsed to the RHF wave function. The BD(T) method has been shown to be problematic[34] in the characterization of several radicals subject to symmetry breaking and the less costly CCSD(T) method appears to be more suitable. Although the R and UCCSD(T) equilibrium geometries of ozone differ in their absolute energies by 6 Kcal/mole, both methods provide a correct description of the region of the PES encompassing both ozone and the concerted TS structure as shown in the next section.

Reliability of the DFT methods is further assessed by a comparison of UDFT and UQCISD results from characterization of the two diradical intermediates $CH_2CH_2O_3(2)$ and $CH_2CH_2O_3(3)$ [with a 6-31+G(d) basis] from the stepwise and partial ozonolysis pathways R2 and R3. Geometry optimization with both UQCISD and UBH&HLYP succeeded in locating the equilibrium structures of the two diradicals. Geometry optimization of $CH_2CH_2O_3(2)$ with both UBLYP and UB3LYP collapsed to the closed-shell ozonide structure. Geometry optimization of $CH_2CH_2O_3(3)$ with UBLYP also

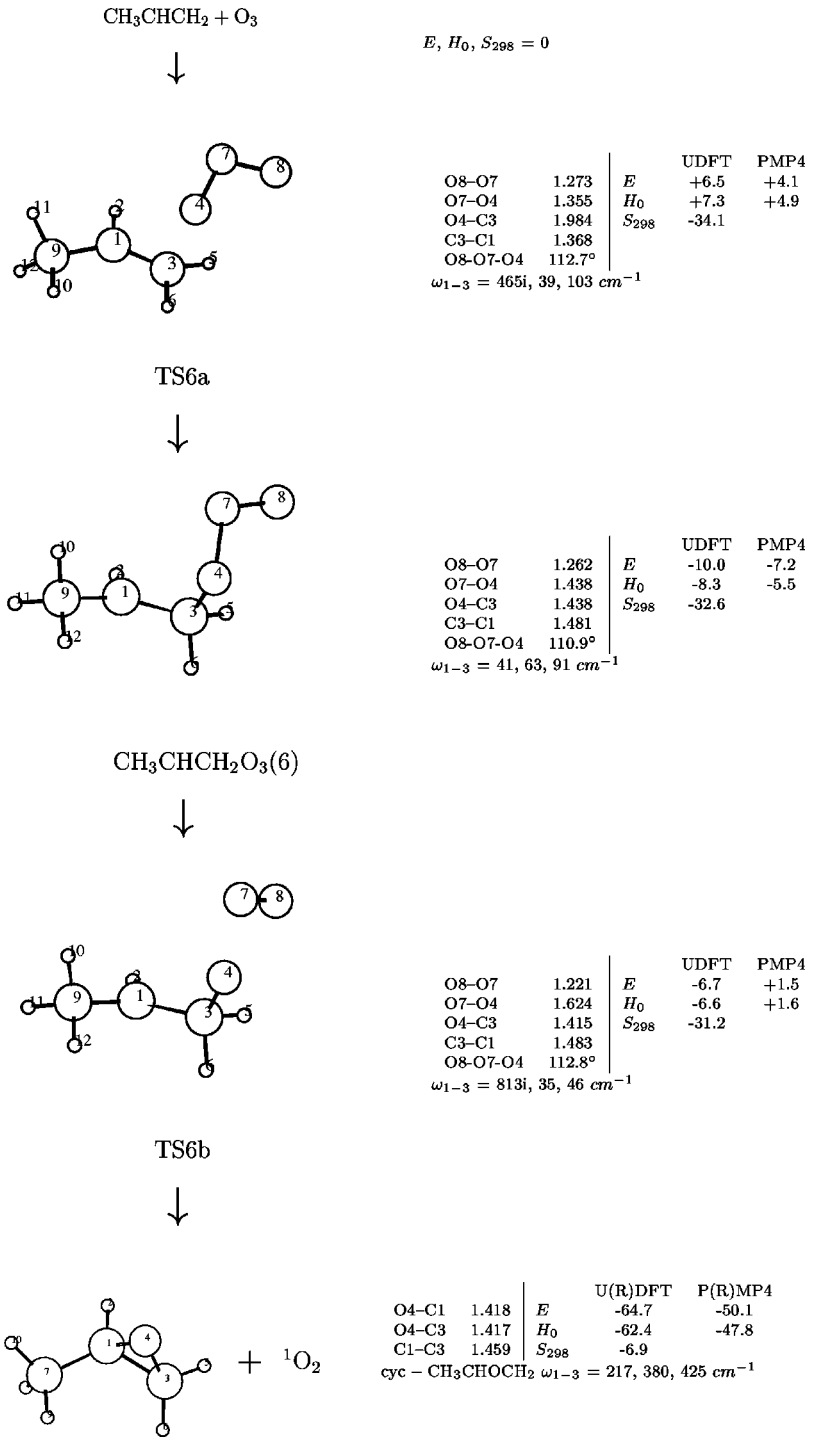

FIG. 6. Partial propene ozonolysis: $CH_3CHCH_2 + O_3 \xrightarrow{TS6a} CH_3CHCH_2O_3(6) \xrightarrow{TS6b}$ cyc-CH_3CHO $CH_2 + {}^1O_2$.

failed to converge while UB3LYP converged to a geometry comparable to that for UBH&HLYP. It is conjectured that the inclusion of larger amount of Hartree–Fock exchange in the BH&HLYP functional results in a greater propensity for spin-symmetry breaking, thereby enabling the location of the equilibrium structure of $CH_2CH_2O_3(2)$ in the vicinity of a closed shell structure. The UBH&HLYP and UQCISD geometries and the three lowest harmonic vibrations (see Appendix) for the two diradicals are in qualitative agreement. The largest absolute deviation of the geometric data occurs in the O9-C2 bond length in $CH_2CH_2O_3(2)$ but the relative error is small. The degree of spin contamination of the UHF and UBH&HLYP solutions for the two diradicals are considerably larger than that for ozone. Nonetheless the T_1 values of the UCCSD wave functions for the diradicals (0.028, 0.029) are smaller than that for ozone (0.061) for which UQCISD predicts reasonably accurate geometry and harmonic vibrations. The UQCISD method is therefore expected to be sufficiently accurate for verification of the two diradicals given the size of the systems investigated. Corresponding RCCSD T_1 values were found to be as high as 0.11 and 0.35 for $CH_2CH_2O_3(2)$ and $CH_2CH_2O_3(3)$, respectively. This implies that the RCCSD(T) method is inapplicable to the study of the stepwise and partial pathways.

TABLE II. Summary of BH&HLYP/6-31+G(d) thermochemical and kinetic calculations for $C_2H_4+O_3$. Energies in Kcal/mole.[a]

		$T=235-362$ K			$T=298.15$ K		
		Log A	E_{act}	E_{cor}	ΔH	$\Delta H^{\ddagger}$	$\Delta G^{\ddagger}$
1	$C_2H_4+O_3 \xrightarrow{TS1}$ cyc-$CH_2O_3CH_2$	9.96	17.7	7.1	−57.4	+17.6	+27.5
2a	$C_2H_4+O_3 \xrightarrow{TS2a} CH_2CH_2O_3(2)$	10.84	8.9	5.1	−8.4	+8.4	+17.6
2b	$CH_2CH_2O_3(2) \xrightarrow{TS2b}$ cyc-$CH_2O_3CH_2$	11.90	1.0	0.1	−49.0	+1.2	+2.2
3a	$C_2H_4+O_3 \xrightarrow{TS3a} CH_2CH_2O_3(3)$	10.96	9.7	7.6	−8.2	+9.2	+18.2
3b	$CH_2CH_2O_3(3) \xrightarrow{TS3b}$ cyc-$CH_2OCH_2+{}^1O_2$	13.43	2.2	7.6	−52.5	+1.6	+1.3
Expt.	$C_2H_4+O_3 \rightarrow$products	9.73	5.08±0.33				

[a]Notes: A, Arrhenius preexponential factor (mole^{-1} cm^3 s^{-1} for bimolecular channels). E_{act}, Arrhenius activation energy. E_{cor}, PMP4 corrected activation energies (see text). ΔH, $\Delta H^{\ddagger}$, enthalpy of reaction and activation. $\Delta G^{\ddagger}$, free energy of activation.

Based on the above discussion, BH&HLYP carried out with a spin-symmetry broken solution is considered to be more suitable than B3LYP and BLYP for the present study.

B. Potential energy surface features

The essential structural and energetic data for R1 to R6 are summarized in Figs. 1–6. Thermochemical quantities E, H_0, and S_{298} (see caption to Fig. 1 for definitions) for each stationary point are relative to the alkene+O_3 reactants. The MP4 and DFT relative energies are referenced to the UDFT and PMP4 energies of ozone. The CCSD(T) energies in Fig. 1 refer to either U or RCCSD(T)[35] and in Fig. 4 to the RCCSD(T) energy of ozone. The total U(R)DFT, P(R)MP4, and U(R)CCSD(T) energies are provided in the Appendix and corresponding spin contamination data of the DFT and UHF wave functions is included as the expectation value of the spin operator S^2. The energy changes and barrier heights for each reaction step are given in Tables II and III along with the corresponding values of Log A and the activation energy.

1. Concerted ozonolysis

For the concerted ozonolysis of ethene (Fig. 1), the DFT value of H_0 (zero-temperature enthalpy) for cyc-$CH_2O_3CH_2$ yields an exothermicity for R1 of −57.4 Kcal/mole, in reasonable agreement with the MP4 value of −57.0 and the U and RCCSD(T) values of −54.1 and −48.1. The DFT value of the zero-temperature activation enthalpy $\Delta H_0^{\ddagger}$, +17.6 Kcal/mole (H_0 of TS1), is substantially lowered to +7.0 by PMP4 and to +7.6 and +8.9 by R and UCCSD(T). These predictions are higher than the previous CCSD(T)/6-311G(2d,2p)//CASSCF/6-31G(d) value of 5.0.[7] The DFT geometry of TS1 is in qualitative agreement with the reported CASSCF/6-31G(d) results but the calculated C–O bond distance is longer by 0.151 Å. Further discussion of these discrepancies from the previous calculations is provided in the Appendix.

The concerted ozonolysis of propene involves more than one possible channel. The transition structure for the lower energy channel (Fig. 4) is found to have the central O atom assuming an ''anti''-orientation with respect to the methyl group. The DFT value of $\Delta H_0^{\ddagger}$, +16.5 Kcal/mol, is lowered to +5.3 by PMP4 and +5.5 by RCCSD(T). The lowering of the activation energy from R1 to R4 is in accordance with the experimental observation of a generally lower barrier height for the ozonolysis of larger alkenes.[11]

2. Stepwise ozonolysis

For the stepwise ozonolysis of ethene (Fig. 2), the $\Delta H_0^{\ddagger}$ of the two consecutive steps R2a and R2b (Fig. 2) are predicted to be +8.4 and +1.2 Kcal/mole by DFT. The first step is the formation of the C4–O5 bond and the lengthening of the adjacent O5–O8 bond and the alkenic double bond. The nearly zero barrier for R2b is consistent with its being a ring-closure reaction involving the formation of a single bond (O9–C2) in the transition from the open-shell TS2b to the closed-shell cyc-$CH_2O_3CH_2$. MP4 reduces the DFT bar-

TABLE III. Summary of BH&HLYP/6-31G(d) thermochemical and kinetic calculations for $CH_3CHCH_2+O_3$. Energies in Kcal/mol.[a]

		$T=235-362$ K			$T=298.15$ K		
		Log A	E_{act}	E_{cor}	ΔH	$\Delta H^{\ddagger}$	$\Delta G^{\ddagger}$
4	$CH_3CHCH_2+O_3 \xrightarrow{TS4}$ cyc-$CH_3CHO_3CH_2$	9.40	16.9	5.7	−58.6	+16.5	+27.5
5a	$CH_3CHCH_2+O_3 \xrightarrow{TS5a} CH_3CHCH_2O_3(5)$	10.08	7.1	3.1	−9.1	+6.4	+16.8
5b	$CH_3CHCH_2O_3(5) \xrightarrow{TS5b}$ cyc-$CH_3CHO_3CH_2$	12.14	0.5	0.3	−53.5	−0.1	+1.3
6a	$CH_3CHCH_2+O_3 \xrightarrow{TS6a} CH_3CHCH_2O_3(6)$	10.58	8.1	5.7	−8.5	+7.3	+17.1
6b	$CH_3CHCH_2O_3(6) \xrightarrow{TS6b}$ cyc-$CH_3CHOCH_2+{}^1O_2$	13.51	2.3	7.7	−54.1	+1.7	+1.4
Expt.	$CH_3CHCH_2+O_3 \rightarrow$products	9.57	3.77±0.22				

[a]See footnotes to Table I.

rier for R2a by 3.8 Kcal/mole while CCSD(T) increases it by 2.9. The positive DFT barrier of R2b is reduced to −2.6 and −0.7 by MP4 and CCSD(T).

For TS2a CCSD(T) predicts E (+10.2 Kcal/mole) to be 4.1 higher than that for TS1 while MP4 predicts E to be 0.7 lower. This discrepancy implies a different order of the barrier heights for the two competing pathways for ethene ozonolysis. This could be the result of the different capability of these methods to correct spin contamination of TS1 and TS2a for which $\langle S^2\rangle_{\mathrm{uhf}}$ varies from 1.1067 to 1.2173. Thus the issue of the choice of the predictions of MP4 versus CCSD(T) is raised. R2a is predicted by CCSD(T) to be nearly thermoneutral with a H_0 of −0.5 Kcal/mole for $CH_2CH_2O_3(2)$ while both MP4 and DFT predict greater exothermicity and hence greater stability for the intermediate. Values for the kinetic stability of $CH_2CH_2O_3(2)$, as measured by the barrier to R2a in the reverse direction, are in good agreement [+9.5 vs +11.7 Kcal/mole for MP4 and CCSD(T)] but are much lower than the DFT value of +16.2. The negative barrier for R2b results from the sensitivity of the minute energy difference between TS2b and $CH_2CH_2O_3(2)$ to structural changes on going from the DFT PES to that of MP4 or CCSD(T) as implied by a difference of 0.1 Å between DFT and UQCISD in the O9–C2 bond length (Appendix: Table IV). A PMP4//DFT energy profile for R2b is given in the Appendix to further characterize the reaction pathway in the vicinity of TS2b.

The stepwise ozonolysis of propene involves more than one possible channel. In the transition structure of the lower energy channel (Fig. 5), O_3 attacks from an "anti"-orientation of the central O atom on the terminal alkenic carbon atom in TS5a. MP4 predicts +3.4 Kcal/mole for the $\Delta H_0^{\ddagger}$ of R5a which is 3.7 lower than the barrier for R2a. Expectation of a minute barrier for R5b, a ring closure rearrangement of $CH_3CHCH_2O_3(5)$ to form the propene ozonide, is in accordance with the DFT $\Delta H_0^{\ddagger}$ of +0.4 Kcal/mole which MP4 predicts to be −2.1. The two values of H_0 for TS5b are in good agreement with a difference of 0.2 Kcal/mol, much smaller than the difference of 2.3 between the values for $CH_3CHCH_2O_3(5)$. Like R2b, the negative barrier for R5b is caused by the difficulty in refinement of a minute energy difference at a higher level of theory.

3. Partial ozonolysis

For the partial ozonolysis of ethene (Fig. 3), DFT and MP4 predict comparable exothermicity for the formation of the intermediate diradical $CH_2CH_2O_3(3)$ (−7.8 and −4.6 Kcal/mole) and barrier height (+9.2 and +7.1). In contrast, CCSD(T) predicts a greater barrier height (+13.3) and nearly zero exothermicity (−0.6). The discrepancy between MP4 and CCSD(T) over the stability of $CH_2CH_2O_3(3)$ is similar to the situation in R2a in that the barrier for R3a in the reverse direction, and hence the kinetic stability of the intermediate diradical, are in close agreement (+11.7 versus +13.9).

In R3b, TS3b corresponds to the dissociation of $CH_2CH_2O_3(3)$ to a highly reactive ethylene oxy radical CH_2CH_2O and singlet molecular oxygen. $\Delta H_0^{\ddagger}$ of R3b obtained from DFT, MP4, and CCSD(T) are +1.6, +7.0, and −2.1 Kcal/mole. The sharp change of spin contamination for the UHF wave function from $CH_2CH_2O_3(3)$ to TS3b ($\langle S^2\rangle_{\mathrm{UHF}} = 1.0399 \rightarrow 1.5410$) likely contributes to the large discrepancy between the MP4 and CCSD(T) values. UCISD and UQCISD geometry optimizations of $CH_2CH_2O_3(3)$ are provided in the Appendix.

TS3b correlates with either two triplets or two singlets and the triplet CH_2CH_2O plus triplet molecular oxygen product channel is favored over the singlet+singlet channel by 21.3 and 8.9 Kcal/mole for MP4 and CCSD(T). Both singlet and triplet CH_2CH_2O are highly unstable at more than 50 Kcal/mole above oxirane but rearrangement of triplet CH_2CH_2O to the closed-shell oxirane is spin-forbidden and singlet CH_2CH_2O is expected to spontaneously collapse to the closed-shell oxirane. However, it is not clear whether TS3b would proceed to the higher energy product channel to any significant extent. Formation of oxirane through a singlet–triplet transition of CH_2CH_2O is also possible as the two states are found to have similar geometries and their energy difference is small (0.7–3.3 Kcal/mole). We have located the transition structure linking $CH_2CH_2O_3(3)$ directly to a product channel of ethylene oxide and singlet molecular oxygen through a concerted dissociation of the O5–O8 bond and formation of a C2–O5 bond. This structure has a plane of symmetry containing C–C–O–O–O and is above TS3b by 0.4 and 1.5 Kcal/mole for MP4 and CCSD(T). However, we could not locate the intermediate linking this transition structure to $CH_2CH_2O_3(3)$. For simplicity, we present cyc-$CH_2OCH_2 + {}^1O_2$ as the product channel of R3b assuming rearrangement of CH_2CH_2O to the epoxide.

The partial ozonolysis of propene involves more than one possible channel. In the transition state of the lower energy channel (Fig. 6), O_3 attacks at the terminal alkenic C atom in TS6a. The $\Delta H_0^{\ddagger}$ of R6a is predicted to be +7.3 and +4.9 Kcal/mol by DFT and MP4. The $\Delta H_0^{\ddagger}$ for R6b, the dissociation of the O–O bond to form molecular oxygen (+1.7 and +7.1) is very similar to the corresponding values for R3b. TS6b links the product channels of propenyl oxyl diradical CH_3CHCH_2OO and molecular oxygen. No lower energy transition structure for a concerted O–O dissociation and C–O bond formation leading to an epoxide and $^1O_2$ could be found. The product channel of R6b is shown to be an epoxide (methyl oxirane) and $^1O_2$.

C. Rate constant data

In Tables II and III the computed values of Log A and the activation energy are compared to the experimental values of Herron and Huie[30] over the temperature range 235–362 K. Both the DFT activation energy, E_{act}, and the PMP4//DFT corrected activation energy, E_{cor}, are shown. The alkene–ozone van der Waals complexes are omitted for the concerted channel although the complex in R1 was characterized by spectroscopic measurement and estimated by theoretical calculations[36] to be bound by 0.74 Kcal/mole. In the absence of tunneling, the existence of a prereactive complex in a bimolecular reaction does not affect its A factor and activation energy under high pressure conditions. Pressure

TABLE IV. Comparison of UQCISD, UBH&HLYP, and UB3LYP results [with a 6-31+G(d) basis set] for $CH_2CH_2O_3(2)$ and $CH_2CH_2O_3(3)$.

	$CH_2CH_2O_3(2)$			$CH_2CH_2O_3(3)$		
	UQCISD	UBH&HLYP	UB3LYP	UQCISD	UBH&HLYP	UB3LYP
O9–O8 (Å)	1.297	1.267	/	1.291	1.261	1.248
O8–O5	1.493	1.426	/	1.510	1.442	1.591
O5–C4	1.464	1.439	/	1.443	1.423	1.419
O9–C2	2.990	2.880	/			
C4–C2	1.486	1.478	/	1.489	1.480	1.487
O9–O8–O5 (deg)	110.2	110.5	/	111.0	110.7	113.8
ω_1 (cm^{-1})	57	92	/	59	76	64
ω_2	137	141	/	108	126	152
ω_3	153	166	/	148	144	190

TABLE V. UDFT, PMP4, UCCSD(T) energies (a.u.), $\langle S^2\rangle$ and T_1 diagnostics for $C_2H_4+O_3$.[a]

	$\langle S^2\rangle_{DFT}$	E(UDFT)	$\langle S^2\rangle_{UHF}$	E(PMP4)	E(UCCSD(T))	T_1
TS3a	0.9502	−303.8189	1.2353	−303.4387	−303.4274	0.045
TS1	0.5180	−303.8161	1.1067	−303.4411	−303.4372	0.060
TS2a	0.8865	−303.8204	1.2173	−303.4423	−303.4308	0.048
TS3b	1.2060	−303.8422	1.5410	−303.4444	−303.4518	0.057
$CH_2CH_2O_3(3)$	1.0119	−303.8469	1.0399	−303.4577	−303.4505	0.028
$CH_2CH_2O_3(2)$	0.9794	−303.8475	1.0238	−303.4587	−303.4508	0.029
TS2b	0.8282	−303.8463	0.9651	−303.4634	−303.4525	0.033
O_3	0.7529	−225.2971	0.9467	−225.0481	−225.0462	0.061
$^1O_2$	1.0097	−150.2318	1.0229	−150.0456	−150.0616	0.041

[a]Note: Entries from TS3a to TS2b listed in descending order of E(PMP4).

TABLE VI. RDFT, RMP4, RCCSD(T) energies (a.u.) and T_1 diagnostics for $C_2H_4+O_3$.[a]

	RDFT	RMP4	RCCSD(T)	T_1
C_2H_4	−78.5349	−78.3997	−78.4008	0.011
O_3	−225.2759	−225.0743	−225.0557	0.029
TS1	−303.8084	−303.4669	−303.4489	0.020
$CH_2CH_2O_3(2)$				0.11*
$CH_2CH_2O_3(3)$				0.35*
cyc-CH_2OCH_2	−153.7006	−153.4783	−153.4757	0.011
cyc-$CH_2O_3CH_2$	−303.9310	−303.5463	−303.5408	0.016

[a]Note:* Obtained from single point RCCSD/6-311+G(2d,p) calculation.

TABLE VII. UDFT, PMP4 energies (a.u.) and $\langle S^2\rangle$ for $CH_3CHCH_2+O_3$.[a]

	$\langle S^2\rangle_{DFT}$	E(UDFT)	$\langle S^2\rangle_{UHF}$	E(PMP4)
TS6a	0.9385	−343.1151	1.2210	−342.6656
TS4	0.5259	−343.1109	1.0981	−342.6676
TS6b	1.2121	−343.1366	1.5387	−342.6698
TS5a	0.8609	−343.1169	1.1988	−342.6700
$CH_3CHCH_2O_3(6)$	1.0147	−343.1415	1.0422	−342.6837
$CH_3CHCH_2O_3(5)$	0.9744	−343.1427	1.0244	−342.6857
TS5b	0.8626	−343.1420	0.9854	−342.6890

[a]Note: Entries from TS6a to TS5b listed in descending order of E(PMP4).

TABLE VIII. RDFT, RMP4, RCCSD(T) energies (a.u.) and T_1 diagnostics for $CH_3CHCH_2+O_3$.

	E(RDFT)	E(RMP4)	E(CCSD(T))	T_1
TS4	−343.1030	−342.6943	−342.6757	0.019
CH_3CHCH_2	−117.8284	−117.6241	−117.6250	0.010
cyc-$CH_3CHO_3CH_2$	−343.2260	−342.7743	−342.7685	0.015
cyc-CH_3CHOCH_2	−192.9968	−192.7064	−192.7035	0.011

independence of ethene ozonolysis is attained at 2–10 torr[37] and we infer that the prereactive complex carries no implications for atmospheric chemistry.

As noted above, the DFT geometries of the singlet diradical intermediates in R2 and R5 are prone to inaccuracies. To resolve the negative barrier heights of R2b and R5b at the PMP4//DFT level, the correction to E_{act} is evaluated as the difference between the DFT and PMP4 values of E for TS2b and TS5b only. Realistic estimates of the rate constants for the stepwise channel would require application of variational transition state theory which entails location of the peak of free energy over the reaction coordinate. However, R2a and R5a should remain the rate-determining steps given their considerably larger barrier heights. The E_{cor} for R3a and R3b are identical and the E_{cor} for R6a is smaller than that for R6b. However, R3a and R6a are the rate-determining steps of the partial ozonolysis mechanism because of the substantially greater A factors of R3b and R6b.

Estimates of the barrier to the interconversion between $CH_2CH_2O_3(2)$ and $CH_2CH_2O_3(3)$ were made. It was concluded that the maximum barrier height lies above TS3b and TS2b and does not interfere significantly with R2b and R3b.

On comparison of E_{cor} for R1, R2a, and R3a to the experimental value of 5.08 Kcal/mole and R4, R5a, and R6a to the experimental value of 3.77, R2a ($E_{cor}=5.1$) and R5a ($E_{cor}=3.1$) of the stepwise mechanism stand out as best matching the experimental values. However, significant discrepancies between A factors of R2a and R5a with the experimental values rule out the stepwise mechanism as the dominant one. Because A factors deduced using empirical methods[38] are generally qualitatively correct, the agreement of the A factors for R1 and R4 overrides the agreement of the E_{act} for R2a and R5a which appears to be fortuitious. Furthermore, the change in E_{cor} from R1 (7.1) to R4 (5.7) matches that for the experimental values. Subtraction of 2.0 Kcal/mole from E_{cor} of R1 and R4 gives 5.1 and 3.7 Kcal/mole and brings both the A factor and activation energy of the concerted mechanism into agreement with experiment.

UCCSD(T)//DFT gives E_{act} of 9.0, 11.8 and 13.6 Kcal/mole for R1, R2a, and R3a and thus correctly predicts the concerted mechanism as the primary pathway for ethene ozonolysis. A larger correction of -4.0 Kcal/mole is required to obtain agreement with experiment. RCCSD(T)//DFT gives a more accurate estimate of E_{act} of 7.7 for R1 and 5.9 for R4. The better accuracy of RCCSD(T) is in accord with the smaller T_1 values (0.020, 0.019) of the RCCSD wave functions of TS1 and TS4. However, the spacing between the two RCCSD(T) estimates does not match the experimental values as well as PMP4.

V. CONCLUDING REMARKS

The procedure of applying RDFT to locate the transition structure of the concerted pathway in a region where both RDFT and RHF are unstable towards spin-symmetry breaking, followed by PMP4 correction of the RDFT barrier height correctly predicts the trend of the experimentally observed A factors and activation energies in the ozonolysis of ethene and propene. However, difficulties arise in finding a procedure that is capable of providing an evenly accurate characterization across the PES encompassing both the partial diradical transition structure in the concerted pathway and the singlet diradical transition structures and intermediates in the stepwise and partial pathways.

Based on UCCSD(T) and experimental results, we conclude that PMP4//U(R)DFT incorrectly resolves the energy difference between the barriers of the concerted and stepwise pathways. PMP4, unlike other post-Hartree–Fock methods, does not belong to the series of systematically improved models[17] of correlated wave functions [i.e., UCCSD(T) > UQCISD > UCISD > UMP4 > UMP2 > UHF]. UCCSD(T) overestimates the barriers of the concerted pathway compared to PMP4 but correctly identifies the mechanism of ozonolysis. This is probable as PMP4 gives greater error relative to UCCSD(T) in regions where spin contamination is low (and vice versa). Given the large range of spin contamination it is possible that PMP4 fails to resolve the small energy changes from partial diradicals to pure singlet diradicals and hence predicts an incorrect trend of the barriers to the concerted and stepwise pathways. Nonetheless, the PMP4//RDFT procedure should serve as a reliable tool for the treatment of concerted ozonolysis across a series of alkenes. It may therefore provide an alternate to UCCSD(T) for extension of the present study to larger alkenes provided that the PMP4//U(R)DFT errors for the concerted and stepwise transition structures are smaller than the discrepancies from the UCCSD(T) values. Although RCCSD(T) was shown to be more accurate than UCCSD(T) for the estimation of the barrier height for the concerted pathway it is inapplicable to the stepwise pathways which require UCCSD(T). Moreover, the use of a combination of R and UCCSD(T) does not necessarily provide more accurate predictions of the *relative* barrier heights for the concerted and stepwise pathways.

The stepwise and partial mechanisms (R2, R3 and R5, R6) have an entropic advantage over the concerted mechanism. Adjusting E_{act} at PMP4//DFT for R2a and R3a to the same energy levels relative to the adjusted E_{act} of R1 (5.1 Kcal/mole) according to CCSD(T)//DFT, the series of E_{act} for R1, R2a, and R3a are set to 5.1, 7.9, and 9.7 Kcal/mole, respectively. At a temperature of 362 K (the upper limit in the experiments of Herron and Huie[30]) this adjusted set of barrier heights gives a ratio of the rate of R2a to R1 of 0.16 while the ratio of the rate of R3a to R1 is 0.017. Production of epoxide as a major product formed from (liquid phase) ozonolysis is known for alkenes with large steric hindrance.[39] We note that the energy difference between the E_{cor} of R4 and R6a (<0.1 Kcal/mol) is smaller than that between R3a and R1 (0.5 Kcal/mol). It is thus possible that partial ozonolysis could make a significant contribution for larger alkenes at elevated temperatures. However, it must be noted that epoxide formation in the gas phase has been attributed to other reaction pathways. A multistep decomposition pathway leading from the ethylene primary ozonide to a oxirane $+ {}^1O_2$ product channel was reported[7] with a maximum barrier height $+5.4$ Kcal/mole above the $C_2H_4 + O_3$ reactant channel. The small yield of epoxide from gas-phase ozonolysis of butadiene[40] has been assigned to the direct dissociation of the ozonide formed in the first step of the decomposition pathway. Furthermore, formation of a triplet

TABLE IX. PMP4/6-311+G(2*d*,*p*)//BH&HLYP/6-31+G(*d*) reaction path between $CH_2CH_2O_3(2)$ and cyc-$CH_2O_3CH_2$.

	O9–C2 (Å)	$\langle S^2\rangle_{DFT}$	*E*(UDFT) (Kcal/mole)	$\langle S^2\rangle_{UHF}$	*E*(PMP4) (Kcal/mole)
$CH_2CH_2O_3(2)$	2.880	0.9794	−9.7	1.0238	−6.8
IRC	2.792	0.9707	−9.6	1.0203	−6.9
IRC	2.729	0.9607	−9.4	1.0166	−7.1
IRC	2.660	0.9490	−9.3	1.0116	−7.2
TS2b	2.389	0.8282	−8.9	0.9651	−9.8
IRC	1.931	0	−25.3	0.3975	−33.7

diradical intermediate as an alternate to epoxide in the channels R3b and R6b cannot be ruled out.

ACKNOWLEDGMENTS

One of the authors (W-T.C.) acknowledges logistic support provided by Professor Huw O. Pritchard in the preliminary stage of this study. I.P.H. thanks NSERC (Canada) and Wilfrid Laurier University for partial funding of this work.

APPENDIX: TECHNICAL ASPECTS

In this section we discuss some aspects pertinent to the calculations for the concerted and stepwise pathways.

Wave function stability

The total U(R)DFT, P(R)MP4, and U(R)CCSD(T) energies are provided in Tables IV–VI for ethene ozonolysis and Tables VII and VIII for propene ozonolysis. The geometric distortion from the equilibrium structure of cyc-$CH_2O_3CH_2$ induces an instability of the RDFT solution for TS1 towards spin and spatial symmetry breaking and a UDFT solution is found with $\langle S^2\rangle = 0.5181$ (Table V) and an energy lowered by 4.8 Kcal/mole. However, this lowering of the energy by UDFT should not be taken as an improvement over RDFT as UDFT yields a second imaginary frequency of 97 cm^{-1} for TS1 corresponding to a structural distortion from the C_s symmetry of the concerted transition structure. Thus UDFT results in a degradation of the PES in the vicinity of TS1. For both ozone and TS1, the classical barrier height and enthalpy of activation are significantly lower for RDFT than for U(R)DFT at +1.5 and +3.5 Kcal/mole, respectively, and in close agreement with corresponding B3LYP/6-31G(*d*,*p*) values of +1.9 and +3.5 Kcal/mole reported in Ref. 8. Using RMP4 for both ozone and TS1, we obtained a classical barrier for R1 of +4.5 Kcal/mole in good agreement with the PMP4 estimate. Based on the above comparisons between the results of unrestricted and restricted methods, we infer that both the RMP4 methods and RDFT provide a qualitatively correct description of the PES encompassing the concerted dissociation of the closed-shell primary ozonide via a partial diradical TS1 which is absent on the UDFT PES. However, proper characterization of ozone requires an unrestricted method and it was found that UDFT predicts more accurate structures and frequencies.

The RDFT solution for TS4 is also unstable to spin-symmetry breaking and a spin contaminated lower-energy UDFT solution is found (Table VII). Although TS4 (unlike TS1) has no symmetry and is not prone to spatial-symmetry breaking, it is still the case that transition structure optimization with UDFT does not converge to a concerted transition structure.

R2b reaction pathway

Resolving the negative barriers for R2b by MP4 and CCSD(T) also requires a more accurate TS2b structure. The barrier for R2b is expected to be very small and is not easily amenable to an accurate transition structure search. In Table IX we report DFT and PMP4 energies for a series of geometries over a range of O9–C2 bond distances between $CH_2CH_2O_3(2)$ and cyc-$CH_2O_3CH_2$ computed by the intrinsic reaction coordinate (IRC) method. The peak of the DFT energy profile occurs at TS2b, beyond which the energy falls off upon formation of the O9–C2 bond. The fall-off is accompanied by a sharp change in $\langle S^2\rangle_{DFT}$, indicating transition of the DFT solution from a singlet diradical to closed-shell singlet. Onset of the rapid fall-off on the PMP4 profile appears to occur before TS2b is reached and no peak is seen on the entire IRC pathway. Precluding the existence of a peak in the gap between $CH_2CH_2O_3(2)$ and the first point of the IRC pathway, R2b is essentially a reaction without a barrier. Because of their size, $CH_3CHCH_2O_3(5)$ and TS5b are not amenable to the techniques employed above. Thus R5b is assumed to be a barrierless reaction which is highly probable for unimolecular radical–radical ring closure.

Based on the above analysis, an adjustment of the negative barrier of MP4 for both R2b and R5b to a small positive value by omission of the energy differences between DFT and MP4 for $CH_2CH_2O_3(2)$ and $CH_3CHCH_2O_3(5)$ may be justified. However, adjustment of the negative barrier of CCSD(T) for R2b is uncertain as this results in a correction of +5.4 Kcal/mole which is unrealistic.

[1] J. H. Seinfeld and S. N. Pandis, *Atmospheric Chemistry and Physics* (Wiley, New York, 1998).
[2] R. Criegee, Angew. Chem. Int. Ed. Engl. **14**, 745 (1975).
[3] R. Atkinson and W. P. L. Carter, Chem. Rev. **84**, 437 (1984).
[4] O. Horie and G. K. Moortgat, Acc. Chem. Res. **31**, 387 (1998).
[5] J. H. Kroll, S. R. Sahay, J. G. Anderson, K. L. Demerjian, and N. M. Donahue, J. Phys. Chem. A **105**, 4446 (2001).
[6] J. D. Fenske, A. S. Hasson, S. E. Paulson, K. T. Kuwata, A. Ho, and K. N. Houk, J. Phys. Chem. A **104**, 7821 (2000).
[7] J. M. Anglada, R. Crehuet, and J. M. Bofill, Chem. Eur. J. **5**, 1809 (1999).
[8] M. Olzmann, E. Kraka, D. Cremer, R. Gutbrod, and S. Andersson, J. Phys. Chem. A **101**, 9421 (1997).
[9] R. Gutbrod, R. N. Schindler, E. Kraka, and D. Cremer, Chem. Phys. Lett. **252**, 221 (1996).
[10] P. S. Bailey, *Ozonation in Organic Chemistry* (Academic, New York, 1978), Vol. I, p. 23.
[11] R. Atkinson, J. Phys. Chem. Ref. Data **26**, 215 (1997).
[12] D. Cremer, E. Kraka, R. Crehuet, J. Anglada, and J. Grafenstein, Chem. Phys. Lett. **347**, 268 (2001).
[13] Y. Yoshioka, T. Tsunesada, K. Yamaguchi, and I. Saito, Int. J. Quantum Chem. **65**, 787 (1997).
[14] J. Baker, A. Scheiner, and J. Andezelm, Chem. Phys. Lett. **216**, 380 (1993).
[15] J. Tian, K. N. Houk, and F. G. Klarner, J. Phys. Chem. A **102**, 7662 (1998).
[16] J. M. Wittbrodt and H. B. Schlegel, J. Chem. Phys. **105**, 6574 (1996).
[17] W. Chen and H. B. Schlegel, J. Chem. Phys. **101**, 5957 (1994).
[18] H. Nakano, K. Hirao, and M. S. Gordon, J. Chem. Phys. **108**, 5660 (1998).
[19] W. T. Borden and E. R. Davidson, Acc. Chem. Res. **29**, 67 (1996).

[20] M. J. Frisch *et al.*, GAUSSIAN 98, Revision A.7, Gaussian, Inc., Pittsburgh PA, 1998.
[21] Q. Zhang, R. Bell, and T. N. Truong, J. Phys. Chem. **99**, 592 (1995).
[22] J. L. Durant, Chem. Phys. Lett. **256**, 595 (1996).
[23] B. J. Lynch, P. L. Fast, M. Harris, and D. G. Truhlar, J. Phys. Chem. A **104**, 4811 (2000).
[24] J. K. Kang and C. B. Musgrave, J. Chem. Phys. **115**, 11040 (2001).
[25] W.-T. Chan, D. Shen, and H. O. Pritchard, Chem. Commun. (Cambridge) **1998**, 583.
[26] W.-T. Chan, H. O. Pritchard, and I. P. Hamilton, Phys. Chem. Chem. Phys. **1**, 3715 (1999).
[27] P. R. Schreiner and M. Prall, J. Am. Chem. Soc. **121**, 8615 (1999).
[28] V. Polo, E. Kraka, and D. Cremer, Theor. Chem. Acc. **107**, 291 (2002).
[29] T. J. Lee and P. R. Taylor, Int. J. Quantum Chem., Symp. **23**, 199 (1989).
[30] J. T. Herron and R. E. Huie, J. Phys. Chem. **78**, 2085 (1974).
[31] T. Tanaka and Y. Morino, J. Mol. Spectrosc. **33**, 538 (1970).
[32] A. Barbe, C. Secroun, and P. Jouve, J. Mol. Spectrosc. **49**, 171 (1974).
[33] M. L. Leininger and H. F. Schaefer, J. Chem. Phys. **107**, 9059 (1997).
[34] T. D. Crawford and J. F. Stanton, J. Chem. Phys. **112**, 7873 (2000).
[35] A PES may be depicted as R- or U-type as designated by the use of either R or U methods to calculate the diradical and partial diradical stationary points. The diradical TSs and intermediates in R2, R3, R5, and R6 were calculated with UDFT, PMP4, and UCCSD(T) and hence the PESs reported are of U-type. R-type PESs were calculated with CCSD(T) for both R1 and R4 as well as a U-type PES for R1. The relative energy of the closed-shell ozonide from R1 on the CCSD(T) R-type PES is referenced to the RCCSD(T) energy of ozone on a R-type PES and to the UCCSD(T) energy of ozone on a U-type PES. With MP4 only the U-type PESs were calculated for R1 and R4. TS1 and TS4 on the DFT PES were calculated with the RDFT method. However UDFT instead of RDFT was employed to calculate ozone to obtain more accurate geometry and harmonic frequences which are needed for reliable TST calculations. To simplify the analysis, the UDFT energy of ozone was taken as the reference energy for R1 and R4. The Appendix provides some examples of calculations for the R-type PESs with MP4 and DFT.
[36] C. W. Gilles, J. Z. Gilles, R. D. Suenram, F. J. Lovas, E. Kraka, and D. Cremer, J. Am. Chem. Soc. **113**, 2412 (1991).
[37] J. H. Kroll, J. S. Clarke, N. M. Donahue, J. G. Anderson, and K. L. Demerjian, J. Phys. Chem. A **105**, 1554 (2001).
[38] S. W. Benson, *Thermochemical Kinetics* (Wiley, New York, 1976).
[39] Reference 10, p. 197.
[40] F. Kramp and S. E. Paulson, Atmos. Environ. **34**, 35 (2000).